JACS
JOURNAL OF THE AMERICAN CHEMICAL SOCIETY

Article

pubs.acs.org/JACS

Challenges in the Structure Determination of Self-Assembled Metallacages: What Do Cage Cavities Contain, Internal Vapor Bubbles or Solvent and/or Counterions?

Cecile C. Givelet,[†] Paul I. Dron,[†] Jin Wen,[†] Thomas F. Magnera,[†] Matibur Zamadar,[†,⊥] Klára Čépe,[§] Hiroki Fujiwara,[†] Yue Shi,[‡] Michael R. Tuchband,[‡] Noel Clark,[‡] Radek Zbořil,[§] and Josef Michl*[,†,∥]

[†]Department of Chemistry and Biochemistry and [‡]Department of Physics, University of Colorado, Boulder, Colorado 80309, United States

[§]Regional Centre of Advanced Technologies and Materials, Faculty of Science, Department of Physical Chemistry, Palacký University, Šlechtitelů 27, Olomouc 783 71, Czech Republic

[∥]Institute of Organic Chemistry and Biochemistry, Academy of Sciences of Czech Republic, Flemingovo nám. 2, 16610 Prague, Czech Republic

Supporting Information

ABSTRACT: Proving the structures of charged metallacages obtained by metal ion coordination-driven solution self-assembly is challenging, and the common use of routine NMR spectroscopy and mass spectrometry is unreliable. Carefully determined diffusion coefficients from diffusion-ordered proton magnetic resonance (DOSY NMR) for six cages of widely differing sizes lead us to propose a structural reassignment of two molecular cages from a previously favored trimer to a pentamer or hexamer, and another from a trimer to a much higher oligomer, possibly an intriguing tetradecamer. In the former case, strong support for the reassignment to a larger cage is provided by an observation of a slow reversible transformation of the initially formed cage into a smaller but spectrally very similar one upon dilution. In the latter case, freeze-fracture transmission electron micrographs demonstrate that at least some of the solutions are colloidal, and high-resolution electron transmission and atomic force microscopy images are compatible with a tetradecamer but not a trimer. Comparison of solute partial molar volumes deduced from measurement of solution density with volumes anticipated from molecular models argues strongly against the presence of large voids (solvent vapor bubbles) in cages dissolved in nitromethane. The presence of bubbles was previously proposed in an attempt to account for the bilinear nature of the Eyring plot of the rate constant for pyridine ligand edge exchange reaction in one of the cages and for the unusual activation parameters in the high-temperature regime. An alternative interpretation is proposed now.

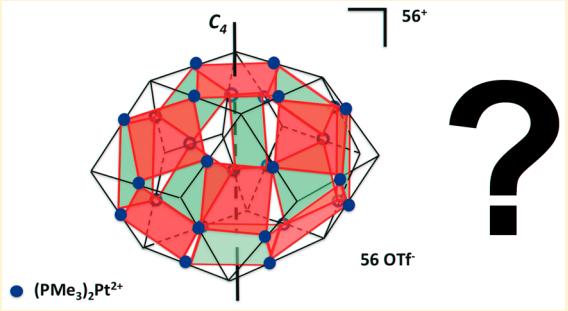

INTRODUCTION

There currently is much interest and activity in metallacages and metallacycles produced by coordination-driven metal ion and ligand self-assembly. Innumerable compounds of this type have been prepared, reported, and discussed in very many review articles, of which we only quote the most recent ones.[1−23] It almost appears that the primary present need is not so much the preparation of additional compounds of this class but rather, a dependable protocol for their secure structural characterization. The most common uncertainty is in the number of building blocks present in the structure; e.g., is it trimeric or hexameric, or perhaps dodecameric? The usual practice of measuring routine mass and NMR spectra leaves too many ambiguities and is clearly insufficient. In recent years, specialized techniques such as traveling-wave ion mobility spectrometry (TWIM-MS) and diffusion-ordered (DOSY) NMR for determination of diffusion coefficients have been used to advantage for unambiguous determination of beautifully complex self-assembled structures.[24−27] Still, obtaining reliably accurate absolute values of the diffusion coefficients is notoriously difficult and we suspect that the DOSY studies likely to be most useful are those in which many similar compounds are measured under identical conditions. In a few cases, solid state structures were obtained by single-crystal X-ray diffraction, but even in these instances, extreme caution is required. Crystals that are analyzed need not be representative of the bulk of the solid material, and structures prevalent in solution need not be the same as those observed in crystals. In most cases only a combination of many methods can provide reasonable assurance that a proposed structure is actually correct, and it is sobering to realize that even then, some residual doubt may remain.

Received: November 17, 2015
Published: April 1, 2016

DOI: 10.1021/jacs.5b12050
J. Am. Chem. Soc. 2016, 138, 6676−6687

The present paper has three objectives. First, we illustrate the challenges involved in cage structure determination by taking a closer look at several cage structures that we have assigned ourselves based on evidence that appeared reasonably convincing, and propose corrections. Second, we ask whether in solution, cages large enough to accommodate several solvent molecules as guests are actually filled with solvent and/or counterions or contain a solvent vapor bubble instead.[28] In view of the small sizes of such cavities, at equilibrium a saturated solvent vapor bubble would often contain only very few solvent molecules or none, and would represent a void. We find no evidence for the presence of such bubbles. Third, we return to the unusual bilinear Eyring plot for the pyridine ligand edge exchange automerization process that was observed earlier[29] in one of the cages we study and was rationalized by postulating the existence of two competing reaction paths, one dominant at low temperatures and the other at high temperatures. It was suggested that the unusually high activation entropy in the latter regime was due to massive solvent reorganization associated with the collapse of a bubble in the transition state, but since the presence of significant voids at equilibrium has now been ruled out, another interpretation of the data is proposed below.

The question about the potential presence of voids in the self-assembled cages is perhaps of the most general interest. For obvious reasons, it could be important in host–guest chemistry, but it has also been raised elsewhere. For instance, it has been proposed that the dynamic process of bubble formation and collapse may represent a mechanism for closing and opening certain cellular ion channels.[30] It is also likely that the formation and collapse of water-free pockets play an important role in protein folding and unfolding,[31,32] and a decades long debate concerning the possible presence of a void in proteins such as interleukin-1β has only relatively recently been settled in favor of its existence.[33]

An immediate response to the title question might be that nature abhors vacuum and that the interior space of a molecule, if accessible and large enough to accommodate several solvent molecules, will always be filled with the liquid solvent that surrounds it. On second thought, however, the answer is less obvious. Surely, at boiling temperature solvent vapor bubbles will form at nucleation sites throughout a solution, and could a cavity not be a favorable nucleation site if its walls are sufficiently solvophobic? Even at temperatures well below boiling, microcapillarity effects could still favor the presence of a bubble.

Closely related issues have received considerable attention from theoreticians. The work was primarily focused on water,[34−40] but other solvents could behave similarly.[41] The structure of a liquid–vapor interface in the presence of a hard wall in the transition region was studied decades ago.[42,43] Molecular dynamics simulations of two paraffin plates immersed in water and located closer than a critical distance apart revealed a spontaneous drying transition, i.e., a cavity-induced liquid–gas phase transition.[44,45] The effect of hydrophobic surface morphology and free energy barriers on the dynamics of capillary evaporation has also been examined.[46−49] The results of a set of molecular dynamics calculations published by our group[29] that predicted bubble formation in a molecular tube unfortunately are wrong due to computer programming errors in the version of the TINK program[50] that was originally used, and could not be reproduced.[51]

So far, to our knowledge there exists no definitive experimental proof for the presence or absence of solvent vapor bubbles in the numerous self-assembled cage molecules that have been synthesized and examined in solution. The experimental data reported in our previous paper[29] provided rather indirect evidence that suggested but certainly did not prove that a bubble might be present in the nitromethane solution of a dodecacation produced by the self-assembly of three tetrapodal connectors **1** with six linkers **2**. Such assembly could lead to the prisms shown in Scheme 1.[52] Circumstantial

Scheme 1. Coordination-Driven Face Directed Self Assembly of 1 and 2 into Possible Oligomeric Prisms 3(n), n = 3−6

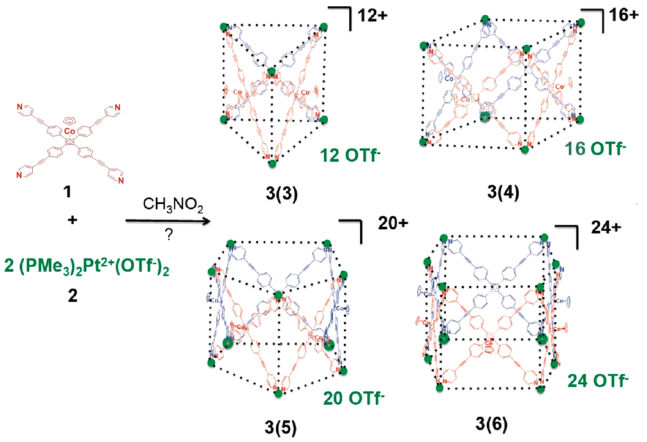

evidence gathered at the time made us propose that the prism formed was the trimer **3(3)** (Chart 1), which has the shape of a large trigonal prismatic tube with three nonpolar walls, six doubly charged vertices and two open ends.

We next define the labels used for all the cages that we consider presently (Chart 1). The first three are prisms assembled from n identical monomeric units, each of which is composed of a tetrapodal connector and two linkers accompanied by four counterions. The prisms are labeled **3(n)**, **4(n)**, and **5(n)**, depending on the nature of the tetrapodal connector used, as specified in Chart 1. Scheme 1 shows the structures **3(3)**−**3(6)** as an example. The degree of oligomerization n in the cages actually produced in the laboratory is not known a priori. In principle, it is also possible that the same monomeric units assemble into structures other than the simple prisms **3(n)**, **4(n)**, and **5(n)**, such as cubes, labeled **3(6c)**−**5(6c)** in Chart 1, or perhaps even larger oligomers. An example of the latter is the rhombic tetradecahedron **4(14h)**, also shown in Chart 1. The positive charges at the corners of the cages are compensated by $CF_3SO_3^-$ or 1-$HCB_{11}Me_{11}^-$ anions present in the nitromethane solution or ion-paired with a corner. Chart 1 also shows the structures of the remaining cages, **6**–**8**, which do not suffer from any ambiguity with regard to oligomerization and do not require the label n. Note that the rectangle **6** is not really a cage and that its shape is far from spherical.

The paper is organized as follows. In the Results section, we briefly describe a greatly improved synthesis of one of the starting materials and then address the issue of cage volumes, both those expected from molecular modeling and those deduced from measurements of solution densities and solute diffusion coefficients. The results show that the cages do not

DOI: 10.1021/jacs.5b12050
J. Am. Chem. Soc. 2016, 138, 6676−6687

Chart 1. Structures of Molecular Cages[a]

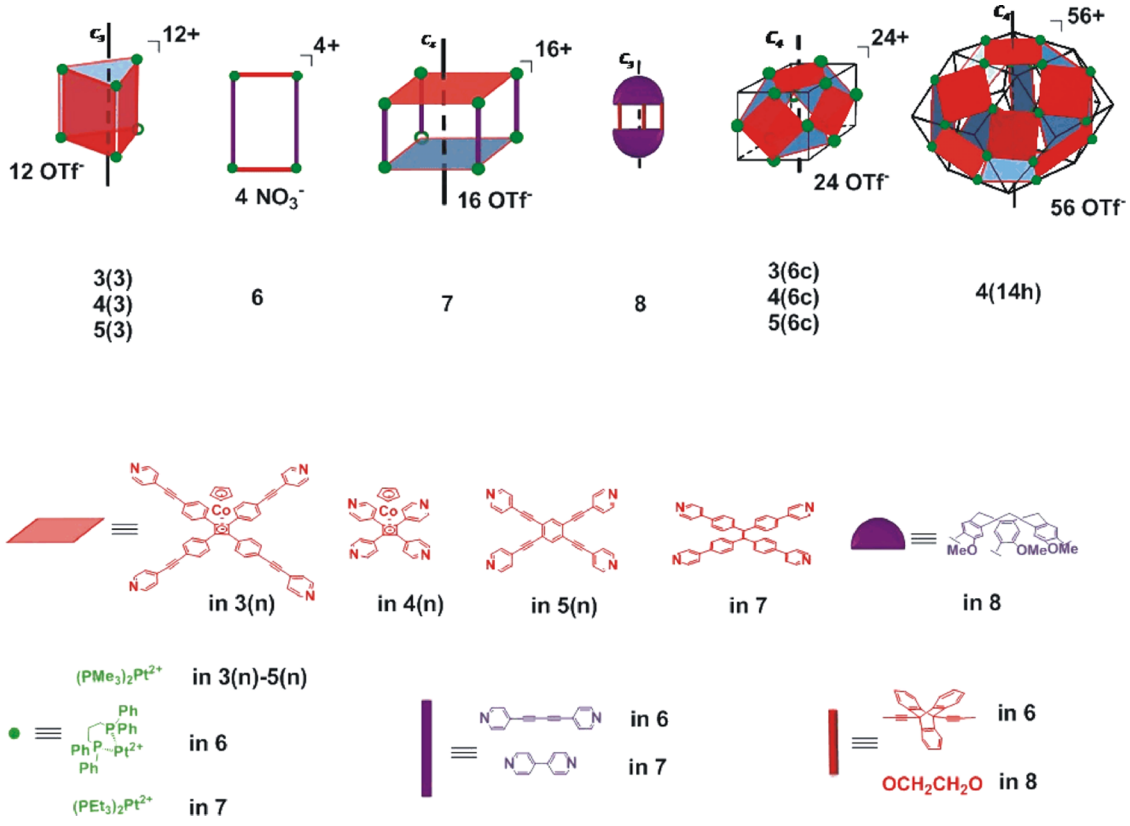

[a]The labels **3**–**8** refer to the nature of the cage faces. The numbers in parentheses, (**3**)–(**6**), refer to the number of faces in a prism (cf. Scheme 1). The number/letter combinations in parentheses refer to other types of oligomers: **c**, a cube, as in (**6c**), and **h**, a tetradecahedron, as in (**14h**). The nature of the links is defined at the bottom.

Scheme 2. Synthetic Path to the Tetrapodal Connector 1

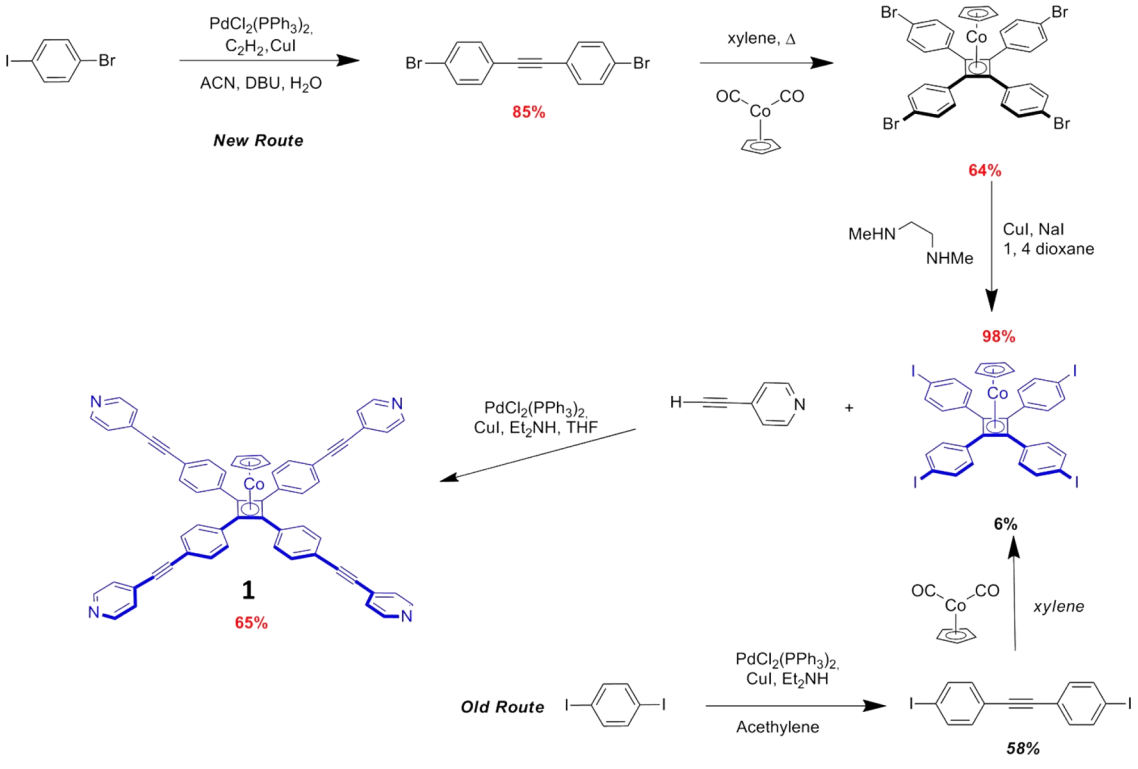

DOI: 10.1021/jacs.5b12050
J. Am. Chem. Soc. 2016, 138, 6676–6687

contain voids and that the degree of oligomerization n in **3**(n), **4**(n), and **5**(n) is higher than the earlier proposed value n = 3. This is further supported by the observation of a slow transformation of **3**(n) into **3**(n'), where $n' < n$. Subsequently, we provide evidence that the solutions of **4**(n) are colloidal. Finally, we return to the measurements of automerization rates in **3**(n) that originally led us to suspect that this cage contains a void. We extend them to additional solvents and describe a more complicated mechanism that avoids unreasonable values of the Eyring parameters. In the Discussion section, we consider all the results and suggest likely structures for the cages **3**(n), **4**(n), and **5**(n).

RESULTS

Cage Preparation. The structures considered are collected in Chart 1. The polycations **3**–**7** were assembled from the constituents shown in Chart 1 and the cryptophane **8**[53] was obtained as a gift. The self-assembly of the cages **3**(n)–**5**(n), where n is not known with certainty but it was previously proposed that n = 3,[52] and the self-assembly of **7**[54] followed literature procedures. That of the rectangle **6** followed a close precedent.[55] The overall yield of the starting material **1** was improved from 3%[52] to 35% by replacing the low-yield dimerization of diiodotolane, difficult to purify from oligomeric byproducts of its preparation, with the efficient[56] dimerization of dibromotolane, prepared easily using DBU as a base,[57] and subsequent transhalogenation[58] (Scheme 2).

Cage Structures and Volumes. There is little or no doubt about the structures of cages **6**–**8**. In contrast, in the absence of X-ray diffraction for a single crystal there is considerable uncertainty about the degree of oligomerization n in **3**(n)–**5**(n). The molecular weight of the polycations is difficult to obtain unambigously from mass spectra and its determination from diffusion-ordered nuclear magnetic resonance (DOSY NMR) data is not straightforward. Therefore, in Scheme 1 (cf. Chart 1) more than one possible product structure is shown as possibly arising in the self-assembly process (n = 3–6), even though the original paper argued in favor of n = 3 in all three cases.[52]

The expected molecular volumes of the cages can be defined in several ways (Table 1). For the total volume of the cage walls plus the counterions, we use V, and without the counterions, we use V'. For the total volume of the cage, including the cavity, we use U if the volume of the counterions (assumed to be located outside the cage) is included and U' if it is excluded. In the absence of voids in the dissolved cages, we expect V to equal the solute partial molar volume. In one extreme limit, if the solvent molecules contained within the cage behave as a part of bulk solvent and do not diffuse with the cage, we expect the cage diffusion constants D to be related to V if there is complete ion pairing and all counterions lie outside, and to V' if there is no ion pairing. In another extreme limit, if the solvent molecules contained within the cage move with the cage, we expect the cage diffusion constants D to be related to U if there is complete ion pairing and to U' if there is none. Intermediate situations are more likely. The extent of ion pairing will be roughly estimated below from a comparison of the D values observed for the cage and the counterion, alone and in the presence of the cage.

Expected Cage Volumes. To estimate the expected cage volumes V, V', U, and U' (Table 1), their molecular structures were first optimized with the UFF[59] and PM6[60] methods with results that differed insignificantly, and the structures of the

Table 1. Calculated and Measured Cage Volumes in nm^3 (cf. Scheme 1 and Chart 1)

	V_{th} [a]	V_{DENS} [b]	U_{th} [c]	U_{th}' [d]	V_{DOSY} [e]
3(1)	2.4	2.13 ± 0.09			
3(3)	7.3	6.40 ± 0.26	9.8	8.8	
3(4)	9.7	8.53 ± 0.34	16.2	15.5	
3(5)	12.2	10.67 ± 0.43	25.2	24.3	
3(6)*	***14.6***	***12.80 ± 0.52***	***33.5***	***32.4***	***33 ± 11***
3(6c)*	***14.6***	***12.80 ± 0.52***	***32.0***	***30.9***	
4(1)	1.6	1.53 ± 0.08			
4(3)	4.9	4.59 ± 0.23	5.2	4.6	
4(4)	6.6	6.12 ± 0.31	7.5	6.8	
4(5)	8.2	7.65 ± 0.38	9.8	8.9	
4(6)	9.8	9.18 ± 0.46	12.3	11.2	
4(6c)	9.8	9.18 ± 0.46	12.0	10.9	
4(14h)*	***23.0***	***21.42 ± 1.07***	***30.1***	***27.5***	***30 ± 10***
5(1)	1.8	1.68 ± 0.05			
5(3)	5.5	5.04 ± 0.15	6.4	5.8	
5(4)	7.3	6.72 ± 0.20	10.2	9.5	
5(5)	9.1	8.40 ± 0.25	14.4	13.5	
5(6)*	***10.9***	***10.08 ± 0.30***	***19.2***	***18.1***	***17 ± 6***
5(6c)*	***10.9***	***10.08 ± 0.30***	***17.0***	***15.9***	
6(1)	2.4	–		–	
6	***4.9***	***4.19 ± 0.29***	***4.9***	***4.7***	***13 ± 6***
7(1)	4.3	–		–	
7*	***8.5***	***8.15 ± 0.49***	***10.2***	***9.5***	***11 ± 3***
8*	***1.4***	***1.11 ± 0.02***	***1.7***	***1.7***	***1.2 ± 0.3***

[a]Cage walls (PM6) and triflate counterions (B97D/SVP). [b]Volume deduced from density measurements. Since the primary quantity measured is density, this volume is proportional to the number of units in the oligomer. [c]Cage walls (PM6), cavity (estimated), and counterions (B97D/SVP). [d]Cage walls (PM6) and cavity (estimated). [e]Volume deduced from measured diffusion constant (Table S7, nitromethane, 298 K, $D/10^{-10}$ m^2·s^{-1}: **3**(n), 1.75 ± 0.27; **4**(n), 1.84 ± 0.33; **5**(n), 2.23 ± 0.35; **6**, 2.62 ± 0.40; **7**, 2.53 ± 0.39; **8**, 5.41 ± 0.27). The D values for the nitromethane solvent can be read off the plots in Figures S5–S16. Within experimental error, volumes determined at other temperatures for four of the compounds were the same as those at 298 K (Tables S1, S2, S4, and S6).

counterions with the B97D/SVP method.[61] The volumes were then calculated using isodensity surfaces obtained with the PM6 method, with the default value of 6.748 e/nm^3 for the density taken from the Gaussian09 program.[62] The volumes listed in Table 1 are simple sums of the volumes of the cage and its triflate counterions, assumed to lie outside. They were only slightly smaller when the counterions were assumed to be tightly paired with the polycations, and the difference was deemed to be within the errors of either estimation.

The calculated values of V and V' within each oligomeric series were proportional to n and can be well approximated by multiplying n with the volume of the monomer **3**(**1**)–**5**(**1**), which contains the tetrapodal connector, two L_2Pt^{2+} binders, and, in the case of V, also four triflate anions. While the calculation of the volumes V_{th} and V_{th}' is fairly unambiguous, the overall calculated volumes U_{th} and U_{th}' that include both the walls and cavity, the former with and the latter without the triflate counterions, are necessarily very approximate, since the boundaries of the cavity are ill-defined in the facets where the cage has a hole in the wall. Even though it cannot be really accurate, in the absence of detailed knowledge we assumed arbitrarily that the boundaries are represented by planes passing through the edges of the squares that define the facets (Chart

DOI: 10.1021/jacs.5b12050
J. Am. Chem. Soc. 2016, 138, 6676–6687

1). The details of the procedure are described in the Experimental Section.

Cage Volumes from Density Measurements. A direct method to measure the molecular volumes is to determine the partial molar volumes from solution density as a function of concentration. Partial molar volumes were determined from densities of solutions of **3(*n*)**–**5(*n*)** and **6**–**8** in nitromethane measured at a series of concentrations, using two different procedures that gave identical results (eqs S1 and S4), and were converted to molecular volumes (V_{DENS} in Table 1). Since the measurement accesses densities rather than volumes directly, the values of V_{DENS} depend linearly on the value of n assumed and the measurement cannot determine which value of n is correct. The V_{DENS} values should agree with V_{th} if the cage does not contain a bubble and with U_{th} if it does. Figure 1 shows a

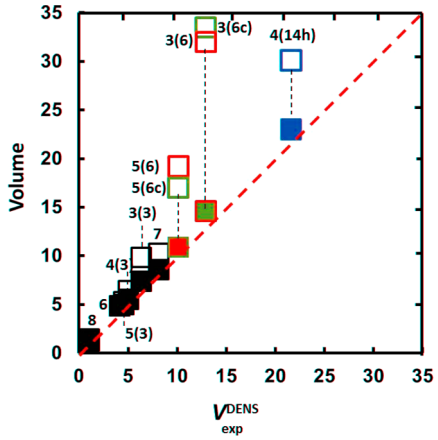

Figure 1. Calculated volumes V_{th} (full squares) and U_{th} (empty squares) plotted against V_{DENS}. For **3(*n*)** and **5(*n*)**, n = 3 (black), n = 6 prismatic (red) and n = 6c cubic (purple), and for **4(*n*)**, n = 3 (black) and n = 14h (green) are shown.

nearly perfect agreement for V_{th} and hardly any for U_{th}, leaving little doubt that the cages do not contain bubbles. In Table 1, we have listed the V_{th} and V_{DENS} values for many choices of n and have marked in boldface italic those that yield the best agreement for V_{DOSY} as discussed below.

Cage Volumes from Diffusion Constants. An experimental method that can be used to estimate the size of the cages is diffusion-ordered NMR (DOSY). The relation between D and V or U is approximated by the Stokes–Einstein equation for macroscopic spherical objects, $D = k_BT/6\pi\eta r$, where k is the Boltzmann constant, T is the absolute temperature, η is the solution viscosity, and r is the radius of the sphere, for which we use either $r = (3V/4\pi)^{1/3}$ or $r = (3U/4\pi)^{1/3}$. An application of this equation to cages **3(*n*)**–**5(*n*)** and **6**–**8**, which are not macroscopic and are at best only approximately spherical, is of doubtful validity, especially in the case of the molecular rectangle **6**, which is not at all spherical and for which a serious misfit can be expected. Still, one can hope that the use of the equation will tie the measured diffusion constants to molecular volumes in an approximate fashion.

The diffusion constants D of the cages **3(*n*)**–**5(*n*)** and **6**–**8** in nitromethane solution were measured using careful precautions to ensure meaningful results (see Experimental Section). The D values given in footnote *e* of Table 1 were converted to V_{DOSY} values listed in Table 1 using the spherical approximation and the Stokes–Einstein equation without any adjustment to determine the radius r as described above and in the Experimental Section. The diffusion constants measured in the same nitromethane solutions for the counterions provide some information about ion pairing. The $D/10^{-10}$ $m^2 \cdot s^{-1}$ values obtained from ^{19}F NMR of the triflate anion were 13.2 ± 0.5 in a solution of pure AgOTf, where the triflate is presumably not significantly ion paired, and 7.9 ± 0.6 in a solution of the triflate of **3**, which is about half way to the value of 1.8 ± 0.3 from the ^1H NMR of the cage **3(*n*)** itself. When two equivalents of $CB_{11}Me_{12}^-$ per Pt^{2+} ion were added, the $D/10^{-10}$ $m^2 \cdot s^{-1}$ value for triflate increased to 12.5 ± 0.4, and it did not change significantly when more $CB_{11}Me_{12}^-$ was added. In spite of the uncertainties introduced by comparing data measured on different nuclei, and not correcting for the small differences in viscosity of the various solutions, one can conclude that on the average, each Pt^{2+} ion of the cage is strongly associated with approximately one counterion and that the $CB_{11}Me_{12}^-$ anion is held more firmly than the triflate anion. If this result holds for all the cages, it would be sensible to use an average of the U_{th} and U_{th}' values when making a comparison with V_{DOSY}, instead of either one individually, but the uncertainty in V_{DOSY} is so huge that it makes no difference whether one or the other value or their average is used.

In Table 1, it is obvious that the values of V_{DOSY} do not agree with V_{th} at all, but agreement with U_{th} can be obtained for suitable choices of n. Those that produce the best fits are shown in bold italic, and the most likely oligomeric structures for the cages **3(*n*)**–**5(*n*)** are marked with an asterisk. The nearly perfect agreement for the cages **7** and **8** where n is not in doubt is encouraging, and the strong disagreement for the rectangle **6** can be blamed on its decidedly nonspherical shape. The V_{DOSY} values for the cages **3(*n*)**–**5(*n*)** are clearly incompatible with the originally proposed trimeric structures, n = 3, and they demand first, that the values of n must be significantly larger than three, and second, that most or all of the solvent molecules contained in the cage diffuse together with the cage. The structures **3(6)** or **3(6c)**, **4(14h)**, and **5(6c)** fit the observations best, but the large margin of error in the V_{DOSY} values makes it impossible to make definitive assignments and structures **3(5)**, **3(7)**, **5(5)**, **5(7)**, and a range of n values in the vicinity of n = 14 for **4(*n*)** are possible as well. We note that a hexameric structure **4(6)** was considered seriously for in the original publication[52] because a corresponding peak was observed in the mass spectrum, but in the end it was felt that this peak would be best attributed to a physical aggregate of two trimers. It now appears that this guess was incorrect. The tetradecameric structure presently proposed for **4(14h)** (Chart 1) was built using the same structural motifs as the smaller oligomers, but other similar and less symmetrical structures are certainly conceivable. The rhombic tetradecahedral structure **4(14h)** has the shape of an oblate ellipsoid with a short (~3 nm) 4-fold axis of symmetry going through the center of a square and two symmetry-related long (~4.3 nm) 2-fold axes perpendicular to it (Figure S1).

Figure 2 provides a graphical presentation of the comparison of the values of V_{DOSY} with V_{th} and U_{th}, once assuming that the structures **3(*n*)**–**5(*n*)** are trimeric as originally proposed (n = 3, black circles), and once assuming that **3(*n*)** and **5(*n*)** are hexameric (n = 6) and that **4(*n*)** is a rhombic tetradecahedron (n = 14h, colored circles) and illustrates the argument.

Direct Evidence Against Trimeric Structure of Cage 3(n). We have noticed that a set of very small peaks in the ^1H NMR spectrum of a 1 mM solution of **3(*n*)**, originally

DOI: 10.1021/jacs.5b12050
J. Am. Chem. Soc. 2016, 138, 6676–6687

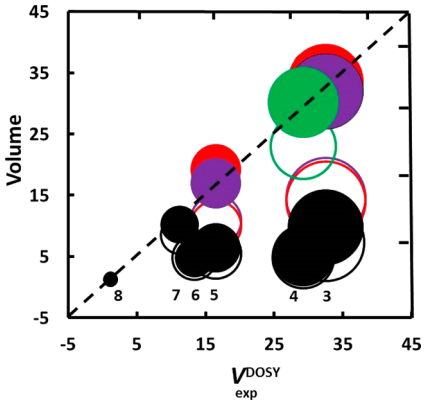

Figure 2. Calculated volumes V_{th} (empty circles) and U_{th} (full circles) plotted against V_{DOSY} for **3**(***n***)−**5**(***n***) and **6**−**8** as indicated at the bottom. For **3**(***n***) and **5**(***n***), n = 3 (black), n = 6 prismatic (red) and n = 6c (cubic, purple), and for **4**(***n***), n = 3 (black) and n = 14h (green) are shown.

attributed to a minute impurity and dismissed, slowly grows over a period of a few days at room temperature or overnight at 60 °C to acquire 10−15% of the intensity of the peaks of the species **3**(***n***) that was originally present essentially exclusively, as determined by NMR integration. Dilution of the sample favors the new species, and a 0.125 mM solution kept at room temperature for 2 days contains 60% of the original species and 40% of the newly formed one. The transformation is reversible and upon evaporation of the nitromethane solvent and adjustment of concentration to 1 mM the original ratio of the two species is restored. The two species exhibit the same pattern of peaks, at only slightly different positions, both in ^{1}H and ^{31}P NMR spectra (Figures S17 and S18). It is particularly significant that in both cases the ^{31}P NMR spectrum contains a single peak, demonstrating the equivalence of all phosphine moieties present in the molecule. We conclude that the original oligomeric cage **3**(***n***) is gradually transformed into a new oligomeric cage **3**(***n***′). The observed enhancement of this transformation upon sample dilution suggests that $n' < n$. There is precedent for reversible conversion of a self-assembled cage into a smaller one upon dilution.[25]

A simultaneous measurement of the diffusion constants of **3**(***n***) and **3**(***n***′) by DOSY ^{1}H NMR provided the values of 1.85 and 2.25 × 10^{-10} $m^2 \cdot s^{-1}$, respectively (Figure S28). Although the individual values of the diffusion constants $D(n)$ and $D(n')$ have limited accuracy, there is no doubt that the latter is larger, and since the NMR spectra suggest that the structures of the two cages are very similar, it follows that $n' < n$. Since the smallest possible cage is trimeric, we conclude that the originally observed cage **3**(***n***) cannot be a trimer as first proposed, but must be at least a tetramer and possibly an even higher oligomer.

The value of 0.82 for the ratio $D(n)/D(n')$ should be quite reliable. If we assume that the Stokes−Einstein relation applies, as suggested by Figure 2, and if we approximate the cage by a sphere of radius r, the volume $V_{DOSY}(n)$ of the original cage and the volume $V_{DOSY}(n')$ of the smaller newly observed cage are related by $V_{DOSY}(n')/V_{DOSY}(n) = [D(n)/D(n')]^3 = 0.55$. An inspection of Table 1 shows that this is close to the ratios expected from the U_{th} (or U_{th}') values for n = 4, n' = 3 (0.60) and for n = 6, n' = 4 (0.48). The ratio expected for n = 5, n' = 4 (0.64) is still relatively close to 0.55, but the ratio for n = 6, n' = 5 (0.75) deviates significantly. Because we do not know that all solvent molecules within the cage move with the cage, nor how many of the counterions are attached to the cage, we cannot choose among the different possible choices of n and n' reliably, especially since the calculated cage volumes U_{th} and U_{th}' of cages with holey walls are in any event only approximate.

Cage Structures. Although we cannot claim that the much better fit observed in Table 1 and Figure 2 for **3**(**6**), **4**(**14h**), and **5**(**6**) compared to the originally proposed **3**(**3**), **4**(**3**), and **5**(**3**), and the independently observed $D(n)/D(n')$ ratio discussed in the preceding paragraph represent a structure proof for these cages, the results exclude the originally proposed trimeric structure for **3**(***n***) and make it highly unlikely for **4**(**3**) and **5**(**3**) as well. Indeed, already the near equality of the D values observed for the large cage **3**(***n***) and the much smaller cage **4**(***n***) using the same value of n for both makes it improbable that these structures have both been assigned correctly as trimers, n = 3. The inadequacy of structure **4**(**3**) is especially striking and we have therefore sought an auxiliary experimental verification of the large size of this cage.

First, the freeze-fracture method (FFTEM) was used in combination with low-resolution TEM. In this procedure, a solution of the cage **4**(***n***) in nitromethane was frozen rapidly by immersion in liquid propane and then fractured and coated with a thin layer of Pt metal. The resulting replica was imaged by TEM (Figures 3 and S19−S23). The images reveal that the

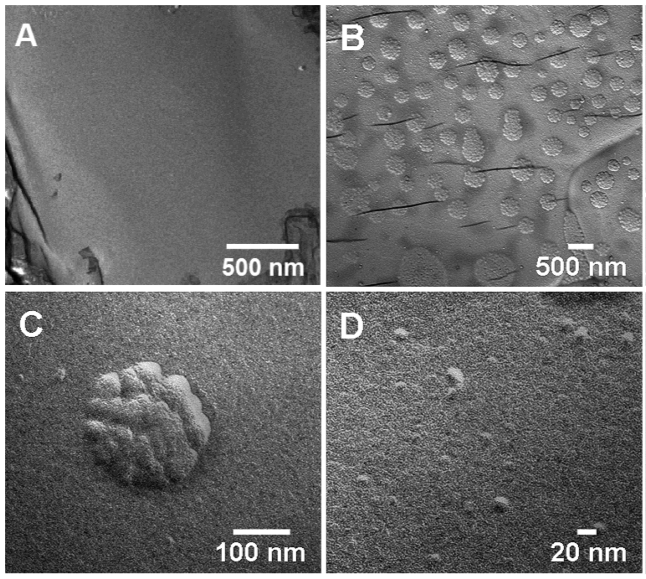

Figure 3. Freeze-fracture TEM images of nitromethane solutions of cage **4**(***n***). (A) Pure solvent; (B,C) solution; (D) solution after extensive centrifugation.

frozen solution is colloidal and contains spherical particles about 200−400 nm in diameter, and that each of these particles is composed of smaller spherical particles about 20−30 nm in diameter. These results were supported by a measurement of dynamic light scattering (DLS), which provided an average particle diameter of 370 nm (polydispersity index 63%) and after sonication, 340 nm (57%), cf. Figure S27. After the solution was centrifuged thoroughly, it no longer produced any dynamic light scattering signal and the larger particles were no longer visible in FFTEM (Figure 3D). Each of the visible smaller particles (8−10 nm) appeared to contain yet smaller particles. The images obtained did not unambiguously identify the size of the smallest constituents.

DOI: 10.1021/jacs.5b12050
J. Am. Chem. Soc. 2016, 138, 6676−6687

Although these results were useful for the recognition of the colloidal nature of our solutions and are compatible with the disc-shaped tetradecamer **4(14h)** shown in Chart 1 and Figure S1, their resolution was insufficient for a clear identification of the number of constituents in the cage. Next, we turned to a combination of high-resolution TEM (HRTEM) and atomic force microscopy (AFM). The size of the TEM molecular images was compatible with the proposed structure **4(14h)** and was much too large for the originally proposed small **4(3)**. EDX showed that the elemental composition of the imaged entities includes Pt and Co and that they are not some random impurities. Still, the results did not appear sufficiently definitive for a proof of structure of **4(14h)**, and have been therefore relegated to the Supporting Information.

Bilinear Eyring Plots. The observation that initially made us suspect that the cage **3(*n*)** contains a void was the bilinear nature of the Eyring plot for the interconversion rates of the two inequivalent edges of its pyridine rings, determined by dynamic ^{1}H NMR,[29] and the unusually highly positive activation entropy in the high-temperature regime (at the time, we considered it most likely that $n = 3$).

We have now confirmed the NMR results and extended them to additional nitroalkane solvents. The Eyring plots for a series of solvents and counteranions were all bilinear (Figure 4, Table 2). The results for the triflate salt agreed with those found earlier, and those obtained in the presence of added 12 equiv of $CsCB_{11}Me_{12}$ were nearly identical with those reported for the $HCB_{11}Me_{11}^-$ salt.[29] We were unable to measure the interconversion rate in **3(*n*′)** by dynamic ^{1}H NMR because the chemical shifts of the protons at the opposite pyridine edges differ too little and the spectrum remains in the fast exchange limit down to the solvent freezing temperature.

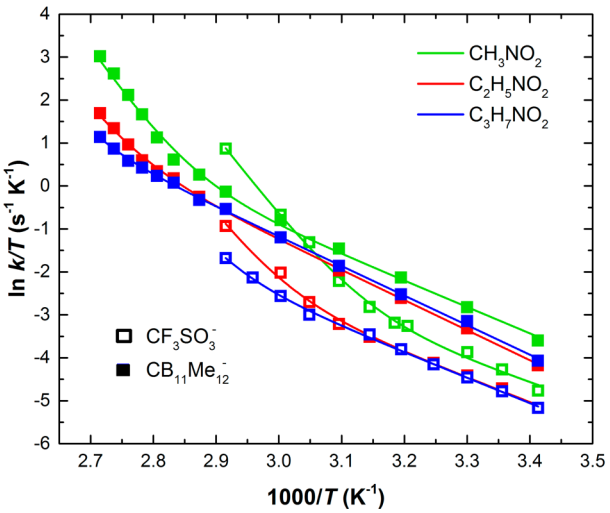

Figure 4. Eyring plots for the automerization reaction of **3(*n*)** + 12 OTf^- (empty squares) and **3(*n*)** + 12 $CB_{11}Me_{12}^-$ (full squares) in nitromethane (green), nitroethane (red), and nitropropane (blue). See text for the origin of the fitting lines.

In the following, we keep the original assumption that the bilinear nature of the Eyring plots reflects the existence of two competing mechanisms for pyridine edge exchange, one dominating at low and the other at high temperatures, and that the low-temperature mechanism is a one-step conformational change in which a pyridine ring rotates around the Pt–N bond, with entirely unexceptional Eyring parameters.

In previous work,[29] we assumed that the high-temperature mechanism also involves a single step (this is referred to below as kinetic model A). The fitting then produced an unusually high activation entropy. Since its proposed rationalization in terms of a bubble present in the cage at equilibrium and collapsing in the transition state is now ruled out, we are forced to assume that the high-temperature mechanism involves one or more intermediates. We first note that the ratio of the diffusion constants of **3(*n*)** and of an inert standard (*o*-carborane, Table S30) remains nearly constant over the temperature range 293–328 K, in which the two linear segments in the Eyring plot meet (T^* = 318 K). This shows that the high-temperature mechanism does not involve the presence of significant amounts of rapidly equilibrating cages of different sizes and suggests that the cage preserves its integrity. This is quite compatible with the slow rate at which the cages **3(*n*)** and **3(*n*′)** equilibrate.

Given this observation, the next simplest assumption (kinetic model B below) is to propose that only one intermediate, **3(*n*)***, is involved and is in rapid equilibrium with **3(*n*)**, with the equilibrium constant given by the ratio of concentrations, $K = [\mathbf{3}(n)^*]/[\mathbf{3}(n)]$. The free energy of **3(*n*)*** is higher by $\Delta G^* = \Delta H^* - T\Delta S^*$. We refer to **3(*n*)*** as the "activated cage". At high temperatures, the exchange of the pyridine edges in this species occurs much faster than in **3(*n*)**, and is responsible for the high rate observed in the NMR experiment. Figure 4 shows that it is possible to fit the observed rate constants with this model B using a stringent least-squares criterion, but the available temperature range is too small and the number of unknown equilibrium and rate parameters too large for the fit to be unique. This overparameterization prevents us from performing a satisfactory statistical analysis. The Eyring parameters derived from the least-squares fitting, especially the activation entropies, now look more reasonable, but their values do not have a statistically meaningful standard error, and the errors are therefore not shown in Table 2. Given this situation, we prefer not to propose a structure for the activated cage **3(*n*)***. Likely candidates are cages that differ from **3(*n*)** in ion pairing and/or by the presence of one or more broken Pt–N bonds. The importance of ion pairing is obvious from the large effect that the choice of counterion and solvent polarity have on the rate constants, and the likely involvement of Pt–N bond breaking is suggested by the large positive values of ΔH^*, consistently close to 20 kcal/mol (Figure 4 and Table 2).

To perform the least-squares simulation using Model B that resulted in the fits shown in Figure 4 we define the rate constant in **3(*n*)** as k and in **3(*n*)*** as k^*, and the corresponding activation parameters as $\Delta H^{\ddagger}$ and $\Delta S^{\ddagger}$ and as $\Delta H^{*\ddagger}$ and $\Delta S^{*\ddagger}$, respectively. The observed rate constant then is given by $k_{obs} = [K/(1 + K)]k^* + [1/(1 + K)]k$, and the expression that was fitted by the least-squares method is given in eq 1, where k_B is the Boltzmann constant and h is the Planck constant:

$$\ln(k_{obs}/T) - \ln(k_B/h) = \Delta S^{\ddagger}/R - \Delta H^{\ddagger}/RT + \ln\{[1 + (\Delta S^*/R)\exp(-\Delta H^*/RT)(\Delta S^{*\ddagger}/\Delta S^{\ddagger}) \times \exp(-\{\Delta H^{*\ddagger} - \Delta H^{\ddagger}\}/RT)] \times [1 + (\Delta S^*/R)\exp(-\Delta H^*/RT)]^{-1}\} \quad (1)$$

In the limit of very low temperatures, this simplifies to

$$\ln(k_{obs}/T) - \ln(k_B/h) = \Delta S^{\ddagger}/R - \Delta H^{\ddagger}/RT \quad (2)$$

DOI: 10.1021/jacs.5b12050
J. Am. Chem. Soc. 2016, 138, 6676–6687

Table 2. Rate and Equilibrium Parameters in Kinetic Models A and B for Pyridine Edge Interchange in 3 and 4 (Enthalpies ΔH in kcal·mol^{-1} and Entropies ΔS in cal·mol^{-1}K^{-1})[a]

		CH_3NO_2[b]			$C_2H_5NO_2$[b]			$C_3H_7NO_2$[b]		
cage and anion	parameter	A	B	T^*[c]	A	B	T^*[c]	A	B	T^*[c]
3(*n*)	$\Delta H^{\ddagger}$	12.4 ± 2.9	9.90	318	12.3 ± 1.9	11.3	323	11.2 ± 1.2	11.7	328
TfO^-	$\Delta H^{*\ddagger}$	34.6 ± 4.8	17.9		24.1 ± 3.6	18.8		19.4 ± 3.9	22.1	
	ΔH^*	–	20.0		–	21.8		–	21.4	
	$\Delta S^{\ddagger}$	−14.4 ± 3.5	−22.4		−14.7 ± 4.4	−18.5		−18.5 ± 5.5	−17.2	
	$\Delta S^{*\ddagger}$	54.6 ± 15.8	43.1		25.8 ± 7.7	34.8		6.4 ± 1.9	36.9	
	ΔS^*	–	21.8		–	34.5		–	36.9	
3(*n*)	$\Delta H^{\ddagger}$	14.1 ± 2.8	12.1	350	14.7 ± 1.9	13.9	357	14.1 ± 1.2	13.6	363
$CB_{11}Me_{12}^-$	$\Delta H^{*\ddagger}$	38.9 ± 5.8	24.4		32.6 ± 3.8	22.7		24 ± 2.4	25.1	
	ΔH^*	–	18.4		–	20.7		–	25.4	
	$\Delta S^{\ddagger}$	−6.6 ± 2.0	−12.5		−5.4 ± 1.6	−7.86		−7.2 ± 2	−8.40	
	$\Delta S^{*\ddagger}$	64.5 ± 16.1	42.2		44.6 ± 8.9	34.0		21.5 ± 5.4	45.3	
	ΔS^*	–	31.6		–	39.1		–	44.5	
4(*n*)[d]	$\Delta H^{\ddagger}$	13.5 ± 2.1			13.4 ± 2.1			–		
TfO^-	$\Delta S^{\ddagger}$	−12.4 ± 4.1			−12.6 ± 4.3			–		

[a]Model A: no intermediates in either temperature regime; $\Delta H^{\ddagger}$ and $\Delta S^{\ddagger}$ from one independent linear fit below T^*, and $\Delta H^{*\ddagger}$ and $\Delta S^{*\ddagger}$ from another independent linear fit above T^*, using eqs 2 and 3, respectively. The square of the correlation coefficient r^2 for each straight line was at least 0.998. Model B: no intermediates in low-temperature regime, one intermediate (activated cage) in high-temperature regime; $\Delta H^{\ddagger}$, $\Delta H^{*\ddagger}$, ΔH^*, $\Delta S^{\ddagger}$, $\Delta S^{*\ddagger}$, and ΔS^* from a simultaneous nonlinear least-squares fit to data at all temperatures, using eq 1. Note that the symbols $\Delta H^{*\ddagger}$ and $\Delta S^{*\ddagger}$ have different significance in the two models. [b]Solvent. [c]Temperature (K) at the intercept of the two straight lines in Model A. [d]For cage **4**(*n*) the Eyring plot is linear at all available temperatures.

and in the limit of very high temperatures, it becomes

$$\ln(k_{obs}/T) - \ln(k_B/h) = \Delta S^{*\ddagger}/R - \Delta H^{*\ddagger}/RT \quad (3)$$

DISCUSSION

The present paper addresses three issues: the reassignment of structures of three self-assembled molecular cages, the presence or absence of voids in such cages, and the bilinear nature of the Eyring plots for cage automerization. We shall discuss the topics in this order.

Structural Reassignment. The re-evaluation of the structures of three of the self-assembled cages requires some knowledge of the volumes associated with the various possible structures, and the estimation of molecular volumes of cages with holey walls involves arbitrary decisions. It does not seem to matter whether PM6 or UFF geometries are used.

The measurements of the diffusion constant produce approximate information on the molecular size. We propose that the original assignment of the structures of cages **3**(*n*)−**5**(*n*) as the trimers **3**(**3**)−**5**(**3**) needs to be replaced by an assignment to higher oligomers. The most likely structures of **3**(*n*) and **5**(*n*) are the hexamers **3**(**6**) and **5**(**6**), but neither the pentamers **3**(**5**) and **5**(**5**) nor the heptamers **3**(**7**) and **5**(**7**) can be excluded. A discovery of a reversible spontaneous transformation of the originally self-assembled cage **3**(*n*) into a smaller cage **3**(*n*′) upon dilution demonstrates particularly clearly that **3**(*n*) cannot be a trimer, $n > 3$. Such spontaneous transformation between other self-assembled cages of different sizes is known.[25]

An egregious discrepancy that definitely requires a structural reassignment has been found for **4**(**3**), which has the second largest V_{DOSY} and the smallest U_{th} of all the prisms. The structure of this cage was misassigned and it is a much higher oligomer than originally proposed. The original assignments were based on less accurate values of the diffusion constants D, but the most important difference is that we now have values for a larger number of molecular cages spanning a larger range of volumes (Figure 2), and this provides an important warning for future work.

The rhombic tetradecahedral structure **4**(**14h**) that we suggest is meant to demonstrate that it is possible to design plausible entities that have the volumes deduced from the observed solution densities and diffusion coefficients, but it probably is just one of many possible oligomeric structures that the constituents might assemble into in nitromethane solution. The real structure remains unproven. The TEM and AFM results are in partial agreement with the expectations for **4**(**14h**). While they are compatible with an oblate disc shape with an expected diameter of ∼4 nm, the observed ∼1 nm height is considerably smaller than the ∼3 nm expected. Perhaps adsorption on a surface distorts the shape of the tetradecahedron, which could well be fairly malleable.

Voids versus Solvent and/or Counterions in Cages. The decision between the presence and the absence of a void in a cage requires some knowledge of the cage volumes in the two cases. The evaluation of the volume denied to the solvent by the solute by measurement of the partial molar volume of the solute is the most direct way to establish the presence or absence of a void in a cage molecule. In its absence, the oligomerization degree n in the self-assembled cage is expected to have no effect on the solute density and the calculated solute volume V_{th} is proportional to n. If a void were present, it would be expected to increase the calculated solute volume to U_{th}, and for a series of similar oligomers such as **3**(*n*), **4**(*n*), or **5**(*n*) the increase would be approximately linear with n as well. The approximate expectations are confronted with the measured molecular volumes in Figure 1. A comparison of the calculated and presently measured molecular volumes, with or without ion pairing, provides no indication that voids are present inside any of the cages.

Our data do not allow us to distinguish whether solvent alone or solvent and counterions fill the free volume of the cages. Anions such as halides,[63,64] nitrate,[65] and azide[66] have been observed to occur inside molecular cages and there

DOI: 10.1021/jacs.5b12050
J. Am. Chem. Soc. 2016, 138, 6676−6687

certainly is enough space inside **3**(*n*), **4**(*n*), and **5**(*n*) to accommodate one or even several counterions. From anion diffusion constants we concluded that in nitromethane solvent at least one $CB_{11}Me_{12}^-$ anion is associated with each vertex, presumably as a weakly held fifth ligand on the platinum dication, in which case it would reside on the outside of the cage. In the same solvent, the triflate anion is clearly held less firmly to a dicationic vertex and ion pairing is less prevalent. Here, the experimental data tell us even less about the possible presence of anions inside the cage. However, in molecular dynamics simulations of the triflate salts in nitromethane solution, we occasionally observed triflate anions inside the cage.

Bilinear Eyring Plots. The conclusion that the cages do not contain bubbles at equilibrium leaves us with a need to find a different explanation for the unusual activation parameters for **3**(*n*) that were obtained previously[29] from the high-temperature part of the bilinear Eyring plots for the rate constant of pyridine edge interchange in a nitromethane-d_6 solution under the assumption that the reaction occurs in a single step (Model A). The highly unusual values of these parameters provided the original motivation for the proposal that this cage contains a vapor bubble.

Such bilinear plots are rare and are normally taken to imply that two competing reaction paths exist, one dominating at the lower and the other at the higher temperatures. A similar bilinear Eyring plot was reported for the encapsulation of small gas molecules in cryptophane cages in chloroform solution and attributed to an unspecified temperature dependence of the kinetic parameters for complexation and decomplexation.[67]

In the low-temperature regime, the results obtained from model A[29] and from the presently developed Model B do not differ much. In the simpler Model A, the activation enthalpy $\Delta H^{\ddagger}$ (~12 and ~15.5 kcal·mol^{-1} in the triflate and the $HCB_{11}Me_{11}^-$ salt, respectively) and activation entropy $\Delta S^{\ddagger}$ (~ −18 and ~ −2 cal·mol^{-1}·K^{-1}, respectively) of the edge interchange process in **3**(**3**) in nitromethane met expectations for a rotation around the Pt−N bond. For instance, $\Delta H^{\ddagger}$ values of 12.5 and 14.1 kcal/mol and $\Delta S^{\ddagger}$ values of −13.9 and −17.2 cal/mol·K^{-1} were reported for the interchange in the PF_6^- salts of Pt-bipyridyl based rectangles and triangles in 1,1,2,2-tetrachloroethane-d_2, respectively.[68] We proposed[29] that the rotation proceeds upon formation of a tight ion pair, and attributed the distinct $\Delta S^{\ddagger}$ values for the triflate and carborate salts to differences in ion pairing: one carborate anion is always paired quite firmly with each Pt dication, whereas the triflate salt may well be partly present as a solvent-separated ion pair. The present results for the diffusion coefficients of the counterions suggest that on the average, each Pt^{2+} center is associated tightly with one counterion.

In contrast to the simple behavior in the low-temperature regime, the high-temperature Eyring parameters are remarkable if they are attributed to a single reaction step (Model A). A $\Delta H^{\ddagger}$ = ~35 kcal·mol^{-1} value is incompatible with a conformational change and suggests a cleavage of one or two ligand-to-metal bonds. A $\Delta S^{\ddagger}$ = ~60 cal·mol^{-1}·K^{-1} value suggests a massive solvent reorganization. Results of a molecular dynamics simulation originally inspired the idea that at high temperatures the reaction proceeds by an associative substitution of pyridine ligands by the counterion (or solvent), breaking one or two Pt−N bonds, and thus opening the cage and causing a collapse of a bubble present in the cage at equilibrium. This would be followed by reclosure during which either side of a freely rotating pyridine ring could end up on the outside of the cage surface.[29] Such reclosure to **3**(*n*) would presumably be identical with the last step of the original synthesis of **3**(*n*) by self-assembly. Even though the computations later turned out to be incorrect due to programming and input errors,[51] they played a heuristic role by hinting at a possible explanation of the odd observed Eyring parameters. The value $\Delta S^{\ddagger}$ = ~60 cal·mol^{-1}·K^{-1} roughly agreed with expectations for the excluded volume entropy of a spherical bubble with a volume equal to that estimated for the internal cavity in **3**(**3**), and encouraged us to propose that at equilibrium a solvent vapor bubble is present.[28,29]

The present finding that solvent vapor bubbles are absent proves that the originally proposed explanation[29] cannot be correct. This led us to suggest that the high-temperature regime the automerization proceeds by a multistep mechanism (kinetic model B) that proceeds through an "activated cage" isomer as an intermediate that most likely differs from **3**(*n*) in ion pairing and probably also Pt−N bond breaking. We have shown that the kinetic data can indeed be fitted to such a mechanism and lead to more reasonable Eyring parameters. Unfortunately, given the large number of unknown equilibrium and kinetic parameters involved in such a scheme, the accessible temperature range is insufficient for a dependable statistical analysis.

An additional possibility is that the kinetic complications are augmented by a temperature dependence of the colloidal nature of the solution. Perhaps the internal structure of the nanoparticles changes abruptly at a certain temperature. We have also considered the possibility that a bubble is only present above a certain temperature, but the density measurements performed on **3**(*n*) and **4**(*n*) gave the same answers at 25, 40, and 70 °C. The diffusion constants measured above and below T^* provide no support for a rapid reversible interconversion between cages of different sizes.

■ CONCLUSION

We disproved the proposed structure **4**(**3**) and concluded that the compound **4**(*n*) self-assembled in nitromethane, where it yields colloidal solutions, is a much higher oligomer. We suggest the rhombic tetradecahedron **4**(**14h**) as an example of a possible structure. We also suggest a reassignment of the published structures **3**(**3**) and **5**(**3**) as **3**(**6**) and **5**(**6**), or possibly **3**(**5**) and **5**(**5**), or conceivably even **3**(**7**) and **5**(**7**). The observed reversible conversion of the cage **3**(*n*) to a smaller cage **3**(*n*′) upon dilution provides particularly strong evidence that $n > 3$.

We have performed direct measurements of molecular volumes that convinced us of the absence of a gaseous solvent vapor bubble in four highly charged self-assembled cages dissolved in nitromethane at temperatures well below the solvent boiling point. The anomalous results of the measurement of kinetic parameters for cage automerization obtained with the simplest kinetic model A and reported earlier in nitromethane and confirmed and extended presently to other solvents need to find another explanation. We have shown that a multistep mechanism (kinetic Model B) for the reaction that dominates at high temperatures is compatible with the observed rate constants and leads to more reasonable values of the Eyring parameters.

■ EXPERIMENTAL SECTION

Synthesis. *cis*-$(Me_3P)_2Pt(OTf)_2$ (**2**)[69] and 1,2-bis(4-bromophenyl)ethyne[57] were prepared according to known procedures. An

DOI: 10.1021/jacs.5b12050
J. Am. Chem. Soc. 2016, 138, 6676−6687

improved preparation of tetrakis[4-iodophenyl]cyclobutadienecyclopentadienylcobalt(I) is described in the Supporting Information.

Density Measurement. Anton Paar 5000 M densitometer with a readability of 1 ppm and automated full-range of viscosity correction and temperature control was used. Several aliquots of different concentrations of prisms **3**(***n***) and **4**(***n***) were prepared in 15 mL vials capped with a hermetical silicone cap wrapped in Teflon tape by weighing with an electro-balance and dissolving in 10 mL of HPLC grade nitromethane. The solutions were degassed by three freeze−pump−thaw cycles and placed under pure helium. The apparatus was closed by attaching a needle to the outlet connection and placing it in a hermetical capped bottle. The system was purged 5 min with helium and degassed pure solvent (3 mL) was introduced to take the first measurement. Between different solutions, the system was purged with helium. Three measurements of 3 mL were performed on each aliquot at 298 K (and in the case of **3**(***n***) and **4**(***n***) also at 313 and 343 K), proceeding from less to more concentrated solutions. Between each set of temperatures, the apparatus was rinsed with nitromethane and then flushed with helium. It was allowed to reach thermal equilibrium between measurements. The densities were treated using eq S1 in Supporting Information. A plot of density as a function of the number of moles of the tube was linear and its slope provided the partial molar volume of the solute (Figure S2). Division by the Avogadro number yielded the volume of a single molecule.

VT-NMR. Spectra were recorded in 1 mM solutions (**6** and **3**(***n***) were 3 mM and 2 mM, respectively, unless stated otherwise) with an Inova 400 spectrometer operating at 400 MHz for ^{1}H and 161.9 MHz for ^{31}P. The ^{1}H chemical shifts are reported relative to the residual protons of CD_3NO_2 (δ 4.33 ppm). An external, unlocked sample of H_3PO_4 was used to reference ^{31}P spectra (δ 0.0 ppm). NMR samples were not degassed. A capillary of nitromethane was used in the NMR tubes of nitroethane and nitropropene solutions, and wet-signals suppression of nitroethane and nitropropane solvents was adopted to improve the signal-to-noise ratio. Temperature-dependent ^{1}H NMR spectra for line-shape analysis were recorded with 400 MHz instruments, over a range spanning the low- to the high-temperature limit. Sample temperatures were calibrated against the displayed sample temperature using the standard method of measuring the shift between the alkyl CH_n vs the OH resonance for either methanol (below ambient) or ethylene glycol (above ambient). Dynamic NMR simulations were performed using the DNMR3 utilities in the Spinworks 2.4 software.[70] The chemical shifts and J coupling constants were accurately determined with the NUMARIT spin-simulation package in Spinworks 2.4, and this was followed by DNMR line shape simulation of the AB spin systems (see Supporting Information). Exchange rate constants k_{obs} were determined at each temperature using the DNMR3 simulation algorithm, and the results were independent of magnetic field strength.

The spectrum shows a nonfirst order AB pattern arising from the inequivalent α and β protons of the pyridine moiety. Computer simulation was used to determine their chemical shifts and J coupling constant before DNMR line shape simulation. The rates were deduced from spectra obtained from 253 to 368 K. They were averaged at selected temperatures after repeating the measurements three times in different NMR tubes. The choice of solvents was limited by solubility and stability of the triflate salts. In the solvents used, no signs of decomposition were observed, except for the slow conversion of **3**(***n***) to **3**(***n***′) noted above.

2D DOSY NMR. Measurements of the diffusion coefficients D were performed with convection compensation using the gradient compensated stimulated echo pulse sequence.[71] In the calculation of the diffusion coefficient, calibrated pulsed field gradient strengths included nonuniform gradient compensation, with a maximum calibrated gradient strength of 55.5 G/cm.[72]

A constant diffusion delay Δ of 0.1 s and δ of 0.003 s was used in all experiments. The DOSY calculations were performed using the multicomponent analysis VNMRJ 3.2A software package, allowing for 2 possible D values for each peak. The concentration of each compound was 1 mM, **6** and **3**(***n***) were respectively 3 mM and 2 mM. The values of D determined by the DOSY experiments were used to calculate the hydrodynamic radii using the Stokes−Einstein equation, $D = k_B T/6\pi R\eta$, where k_B is the Boltzmann constant, T is the absolute temperature, and η is the viscosity of nitromethane (0.0062 g s^{-1} cm^{-1}).

Photoacoustic Spectroscopy. A solution of **3**(***n***) in 1,2-dichloroethane with absorbance of 0.5−1 was irradiated through a 200 mm focusing lens in a quartz cell with a 10 mm optical path length at either 355 nm obtained by third harmonic generation from a 7 ns Nd:YAG laser (10 Hz) or at 308 nm obtained from a XeCl excimer laser (1 Hz). The pulse energy from the Nd:YAG laser was manually changed between 1 and 100 μJ using normal density filters and monitored with a power meter. The excimer laser pulse energy was changed by the modulation of discharge voltage about 10-fold while monitoring the output intensity with a photodiode. Sample solutions were prepared with sonication, stored overnight in the refrigerator, purged by nitrogen for 20 min, filtered by a Teflon membrane filter (Polytetrafluoroethylene Syringe Filter, 0.45 μm, nonsterile, Sterlitech) and continuously flowed by gravity at ∼10 mL/min during the experiment to avoid the accumulation of photoproducts. Transient photoacoustic waves from the solutions of **3**(***n***) and a calorimetric reference (solution of freshly recrystallized tetraphenylethylene for work at 355 nm and pyridazine for work at 308 nm) were detected by a piezoelectric transducer using vacuum grease as the coupling medium and handled with LabVIEW SignalExpress in continuous sample (1-accumulation) acquisition mode. Three to seven sets of data were recorded at each excitation energy. The experiments were carried out at least twice.

FFTEM.[73] A solution of **4**(***n***) in nitromethane (1−2 μL) was placed on a homemade 2 mm × 4 mm sterilized glass (planchette) cell with no prior surface treatment, and covered with another piece of glass to create a sandwich cell. The planchettes were then rapidly quenched by immersion in liquid propane (−190 °C) and fractured in high vacuum by mechanically pulling the glass cell apart at −140 °C. The fractured surfaces were coated with 2 nm of platinum deposited at 45° and then with 25 nm of carbon deposited at 90°. The coated materials were removed from high vacuum and the platinum−carbon replica was freed from the material on the glass cell by action of ethyl acetate solvent. The replica was then placed in the TEM to observe the topography of the fractured plane. FFTEM images can be best understood with the idea that darker regions are angled toward the platinum source, and lighter regions are angled away from it. The TEM instrument used was a Phillips CM (FEI Company, Hillsboro, OR) 10; 100 kV TEM equipped with 1K × 1K Gatan Bioscan digital camera.

HRTEM. Images were obtained using the HRTEM FEI Titan G2 microscope with image corrector. One drop of solution was placed on a copper grid with holey carbon film and dried at room temperature. The accelerating voltage was 80 kV. Images were captured by Gatan BM Ultrascan CCD camera. The microscope is equipped with EDS equipment (Energy Dispersive Spectroscopy, Bruker) for chemical mapping. The aquisition time for collecting of EDS spectra was 15 min.

AFM. Images were obtained using an SPM microscope NTEGRA/NT-MDT. One drop of solution was placed on mica and dried at room temperature. The measurements were performed in air at room temperature in the semicontact mode with Ha-NC tips.

Dynamic Light Scattering (DLS). Intensity autocorrelation was measured on a home-built instrument[74] using a 1 mW 632.8 nm laser and detecting the scattered light at an angle of 30°. Before use, the nitromethane solvent was passed through a filter to remove dust particles. Centrifugation at 108 kg for 20 h caused the DLS signal from the top part of the solution to disappear.

Computational Methods. The volumes of the cages and their triflate counterions were obtained at UFF[59] optimized geometries using the TINK program[50] for the molecular cages. B97D/SVP[61] optimized geometry was used for the anions. The volumes were evaluated from the PM6 isodensity surfaces.[60] The volumes of the cationic cage and the anions were added to obtain the molecular volume in the limit of no ion pairing. In the limit of full ion pairing, which we do not believe to describe reality, the same cage geometry

DOI: 10.1021/jacs.5b12050
J. Am. Chem. Soc. 2016, 138, 6676−6687

was adopted and a triflate anion was added on both sides of each of the six platinum atoms at an O−Pt distance of 3.4−4.0 Å for the three oxygen atoms. This distance and the orientation of the triflate anion were obtained by a B97D/SVP optimization of the model system $[Py_2Pt(PMe_3)_2][TfO]_2$. The Mulliken charges in this model system were −0.7 |e| on the anion and +1.4 |e| on the cation.

The volume of the internal cavity of the cage was approximated as the product of the base area and the height of the prism. To account for the volume occupied by molecules themselves, the edge lengths of the base were corrected by subtracting half the 3.4 Å thickness of the aromatic molecules from the lengths of Pt−Pt edges. The height of the prism was determined as the length of the parallel edges.

■ ASSOCIATED CONTENT

Supporting Information

The Supporting Information is available free of charge on the ACS Publications website at DOI: 10.1021/jacs.5b12050.

Synthesis, details of density and NMR measurements, AFM and TEM images, DLS results, and full text of ref 58 (PDF)

■ AUTHOR INFORMATION

Corresponding Author

*michl@eefus.colorado.edu

Present Address

⊥M.Z.: Department of Chemistry and Biochemistry, Stephen F. Austin State University, Nacogdoches, Texas 75962, United States

Notes

The authors declare no competing financial interest.

■ ACKNOWLEDGMENTS

This work was supported by the National Science Foundation (CHE-1265922 and DMR-1420736) and by the Ministry of Education, Youth and Sports of the Czech Republic (LO1305). J.W. thanks the Chinese Scholar Council (No. 2009619059; Study Abroad Project) for financial support when she was a visiting graduate student from Nanjing University. We are grateful to Drs. Mark O. McLinden and Tara Fortin at NIST, Boulder, for permission to use their densitometer and for assistance in its use; and to Tanja Denike from the company Anton Paar (10250 Timber Ridge Drive, Ashland, Virginia 23005, United States) for subsequently lending us a densimeter. We thank Prof. Peter Stang for a gift of a precursor for **7** and a valuable discussion, and Prof. Thierry Brotin for a gift of **8**.

■ REFERENCES

(1) Cook, T. R.; Stang, P. J. *Chem. Rev.* **2015**, *115*, 7001.
(2) McConnell, A. J.; Wood, C. S.; Neelakandan, P. P.; Nitschke, J. R. *Chem. Rev.* **2015**, *115*, 7729.
(3) Newkome, G. R.; Moorefield, C. N. *Chem. Soc. Rev.* **2015**, *44*, 3954.
(4) Brown, C. J.; Toste, F. D.; Bergman, R. G.; Raymond, K. N. *Chem. Rev.* **2015**, *115*, 3012.
(5) Yoshizawa, M.; Klosterman, J. K. *Chem. Soc. Rev.* **2014**, *43*, 1885.
(6) Castilla, A. M.; Ramsay, W. J.; Nitschke, J. R. *Acc. Chem. Res.* **2014**, *47*, 2063.
(7) Saha, M. L.; Neogi, S.; Schmittel, M. *Dalton Trans.* **2014**, *43*, 3815.
(8) Han, M.; Engelhard, D. M.; Clever, G. H. *Chem. Soc. Rev.* **2014**, *43*, 1848.
(9) Cook, T. R.; Zheng, Y. R.; Stang, P. J. *Chem. Rev.* **2013**, *113*, 734.
(10) Saha, M. L.; De, S.; Pramanik, S.; Schmittel, M. *Chem. Soc. Rev.* **2013**, *42*, 6860.
(11) Harris, K.; Fujita, D.; Fujita, M. *Chem. Commun.* **2013**, *49*, 6703.
(12) Ward, M. D.; Raithby, P. R. *Chem. Soc. Rev.* **2013**, *42*, 1619.
(13) Cook, T. R.; Vajpayee, V.; Lee, M. H.; Stang, P. J.; Chi, K.-W. *Acc. Chem. Res.* **2013**, *46*, 2464.
(14) Smulders, M. M. J.; Riddell, I. A.; Browne, C.; Nitschke, J. R. *Chem. Soc. Rev.* **2013**, *42*, 1728.
(15) Saha, M. L.; Schmittel, M. *Org. Biomol. Chem.* **2012**, *10*, 4651.
(16) Breiner, B.; Clegg, J. K.; Nitschke, J. R. *Chem. Sci.* **2011**, *2*, 51.
(17) Safont-Sempere, M. M.; Fernández, G.; Würthner, F. *Chem. Rev.* **2011**, *111*, 5784.
(18) Chakrabarty, R.; Mukherjee, P. S.; Stang, P. J. *Chem. Rev.* **2011**, *111*, 6810.
(19) De, S.; Mahata, K.; Schmittel, M. *Chem. Soc. Rev.* **2010**, *39*, 1555.
(20) Pluth, M. D.; Bergman, R. G.; Raymond, K. N. *Acc. Chem. Res.* **2009**, *42*, 1650.
(21) Klosterman, J. K.; Yamauchi, Y.; Fujita, M. *Chem. Soc. Rev.* **2009**, *38*, 1714.
(22) Northrop, B. H.; Zheng, Y.-R.; Chi, K.-W.; Stang, P. J. *Acc. Chem. Res.* **2009**, *42*, 1554.
(23) Yoshizawa, M.; Klosterman, J. K.; Fujita, M. *Angew. Chem., Int. Ed.* **2009**, *48*, 3418.
(24) Xie, T.-Z.; Guo, K.; Guo, Z.; Gao, W.-Y.; Wojtas, L.; Ning, G.-H.; Huang, M.; Lu, X.; Li, J.-Y.; Liao, S.-Y.; Chen, Y.-S.; Moorefield, C. N.; Saunders, M. J.; Cheng, S. Z. D.; Wesdemiotis, C.; Newkome, G. R. *Angew. Chem., Int. Ed.* **2015**, *54*, 9224.
(25) Lu, X.; Li, X.; Guo, K.; Xie, T.-Z.; Moorefield, C. N.; Wesdemiotis, C.; Newkome, G. R. *J. Am. Chem. Soc.* **2014**, *136*, 18149.
(26) Sarkar, R.; Guo, K.; Moorefield, C. N.; Saunders, M. J.; Wesdemiotis, C.; Newkome, G. R. *Angew. Chem., Int. Ed.* **2014**, *53*, 12182.
(27) Wang, M.; Wang, C.; Hao, X.-Q.; Liu, J.; Li, X.; Xu, C.; Lopez, A.; Sun, L.; Song, M.-P.; Yang, H.-B.; Li, X. *J. Am. Chem. Soc.* **2014**, *136*, 6664.
(28) Michl, J. In *Non-Covalent Assemblies to Molecular Machines*; Sauvage, J.-P., Gaspard, P., Eds.; Wiley-VCH: Weinheim, Germany, 2010; p 51.
(29) Vacek, J.; Caskey, D. C.; Horinek, D.; Shoemaker, R. K.; Stang, P. J.; Michl, J. *J. Am. Chem. Soc.* **2008**, *130*, 7629.
(30) Roth, R.; Gillepsie, D.; Nonner, W.; Eisenberg, B. *Biophys. J.* **2008**, *94*, 4282.
(31) Liu, P.; Huang, X.; Zhou, R.; Berne, B. J. *Nature* **2005**, *437*, 159.
(32) Sumit, S.; Debenedetti, P. G. *Proc. Natl. Acad. Sci. U. S. A.* **2012**, *109*, 4365.
(33) Matthews, B. W.; Liu, L. *Protein Sci.* **2009**, *18*, 494.
(34) Chandler, D. *Nature* **2005**, *437*, 640.
(35) Ben-Amotz, D. *J. Chem. Phys.* **2005**, *123*, 184504−1.
(36) Choudhury, N.; Pettitt, B. M. *J. Am. Chem. Soc.* **2007**, *129*, 4847.
(37) Frank, H. S.; Evans, M. W. *J. Chem. Phys.* **1945**, *13*, 507.
(38) Ball, P. *Chem. Rev.* **2008**, *108*, 74.
(39) Hummer, G.; Garde, S.; Garcia, A. E.; Pohorille, A.; Pratt, L. R. *Proc. Natl. Acad. Sci. U. S. A.* **1996**, *93*, 8951.
(40) Smeets, R. M. M.; Keyser, U.; Wu, M. Y.; Dekker, N. H.; Dekker, C. *Phys. Rev. Lett.* **2006**, *97*, 088101−1.
(41) Wilhelmsen, Ø.; Bedeaux, D.; Kjelstrup, S.; Reguera, D. *J. Chem. Phys.* **2014**, *141*, 071103.
(42) Percus, J. K.; Kalos, M. H.; Rao, M.; Berne, B. J. *J. Chem. Phys.* **1979**, *71*, 3802.
(43) Kalos, M. H.; Rao, M.; Berne, B. J. *J. Chem. Phys.* **1978**, *68*, 1325.
(44) Huang, X.; Zhou, R.; Berne, B. J. *J. Phys. Chem. B* **2005**, *109*, 3546.
(45) Liu, P.; Harder, E.; Berne, B. J. *J. Phys. Chem. B* **2005**, *109*, 2949.
(46) Luzar, A.; Leung, K. *J. Chem. Phys.* **2000**, *113*, 5836.
(47) Leung, K.; Luzar, A. *J. Chem. Phys.* **2000**, *113*, 5845.
(48) Lum, K.; Luzar, A. *Phys. Rev. E: Stat. Phys., Plasmas, Fluids, Relat. Interdiscip. Top.* **1997**, *56*, 6283.
(49) Leung, K.; Luzar, A.; Bratko, D. *Phys. Rev. Lett.* **2003**, *90*, 1−4.

DOI: 10.1021/jacs.5b12050
J. Am. Chem. Soc. 2016, 138, 6676−6687

(50) Vacek, J.; Michl, J. *New J. Chem.* **1997**, *21*, 1259.
(51) Correction to ref 29: Vacek, J.; Caskey, D. C.; Horinek, D.; Shoemaker, R. K.; Stang, P. J.; Michl, J. *J. Am. Chem. Soc.* **2016**, DOI: 10.1021/jacs.6b04606.
(52) Caskey, D. C.; Yamamoto, T.; Addicott, C.; Shoemaker, R. K.; Vacek, J.; Hawkridge, A. M.; Muddiman, D. C.; Kottas, G. S.; Michl, J.; Stang, P. J. *J. Am. Chem. Soc.* **2008**, *130*, 7620.
(53) Chaffee, K. E.; Fogarty, H. A.; Brotin, T.; Goodson, B. M.; Dutasta, J.-P. *J. Phys. Chem. A* **2009**, *113*, 13675.
(54) Wang, M.; Zheng, Y.- R.; Ghosh, K.; Stang, P. *J. Am. Chem. Soc.* **2010**, *132*, 6282.
(55) Plutnar, J.; Givelet, C.; Buchanan, E.; Lemouchi, C.; Dytrtová, J.; Michl, J., unpublished results.
(56) Harrison, R. M.; Brotin, T.; Noll, B.; Michl, J. *Organometallics* **1997**, *16*, 3401.
(57) Mio, M. J.; Kopel, L. C.; Braun, J. B.; Gadzikwa, T. L.; Hull, K. L.; Brisbois, R. G.; Markworth, C. J.; Grieco, P. A. *Org. Lett.* **2002**, *4* (19), 3199.
(58) Klapars, A.; Buchwald, S. L. *J. Am. Chem. Soc.* **2002**, *124*, 14844.
(59) Rappe, A. K.; Casewit, C. J.; Colwell, K. S.; Goddard, W. A., III; Skiff, W. M. *J. Am. Chem. Soc.* **1992**, *114*, 10024.
(60) Stewart, J. J. P. *J. Mol. Model.* **2007**, *13*, 1173.
(61) Grimme, S. *J. Comput. Chem.* **2006**, *27*, 1787.
(62) Frisch, M. J. et al., *Gaussian 09*, revision B.01; Gaussian, Inc.: Wallingford, CT, 2010.
(63) Graf, E.; Lehn, J.-M. *J. Am. Chem. Soc.* **1976**, *98*, 6403.
(64) Metz, B.; Rosalky, J. M.; Weiss, R. *J. Chem. Soc., Chem. Commun.* **1976**, *3*, 533.
(65) Takezawa, H.; Murase, T.; Resnati, G.; Metrangolo, P.; Fujita, M. *Angew. Chem., Int. Ed.* **2015**, *54*, 8411.
(66) Lehn, J.-M.; Sonveaux, E.; Willard, A. K. *J. Am. Chem. Soc.* **1978**, *100*, 4914.
(67) Chaffee, K. E.; Fogarty, H. A.; Brotin, T.; Goodson, B. M.; Dutasta, J.-P. *J. Phys. Chem. A* **2009**, *113*, 13675.
(68) Tárkányi, G.; Jude, H.; Pálinkás, G.; Stang, P. J. *Org. Lett.* **2005**, *7*, 4971.
(69) Stang, P. J.; Cao, D. H.; Saito, S.; Arif, A. M. *J. Am. Chem. Soc.* **1995**, *117*, 6273.
(70) Marat, K. *Spinworks 2.4 Software*; University of Manitoba, http//www.umanitoba.ca/chemistry/nmr/spinworks.
(71) Jerschow, A.; Müller, N. *J. Magn. Reson.* **1997**, *125*, 372.
(72) Connell, M. A.; Bowyer, P. J.; Bone, P. A.; Davis, A. L.; Swanson, A. G.; Nilsson, M.; Morris, G. A. *J. Magn. Reson.* **2009**, *198*, 121.
(73) Chen, D.; Heberling, M.-S.; Nakata, M.; Hough, L. E.; Maclennan, J. E.; Glaser, M. A.; Korblova, E.; Walba, D.; Watanabe, J.; Clark, N. *ChemPhysChem* **2012**, *13*, 155.
(74) Clark, N. A.; Lunacek, J. H.; Benedek, G. B. *Am. J. Phys.* **1970**, *38*, 575.

DOI: 10.1021/jacs.5b12050
J. Am. Chem. Soc. 2016, 138, 6676−6687